UNIVERSITY OF CALIFORNIA,
IRVINE

OPTIMIZING BOND MULTIVALENCY WITH SPRINGY LINKERS FOR THERAPEUTIC NANOPARTICLES

THESIS

submitted in partial satisfaction of the requirements
for the degree of

MASTERS OF SCIENCE

in Biomedical Engineering

by

Phi Dominh

Thesis Committee:
Assistant Professor Jered Haun, Chair
Associate Professor James Brody
Assistant Professor Chang Liu

2017

DEDICATION

To

my family and friends

in recognition of their love and support

The phoenix must burn to emerge.

Janet Fitch

White Oleander

TABLE OF CONTENTS

LIST OF FIGURES

LIST OF TABLES

ACKNOWLEDGEMENTS

My deepest appreciations go to my committee chair, Assistant Professor Jered Haun. His patience and guidance past three years are the pillars for my strength and desire of research. The memories made will always be remembered fondly.

I would like to thank my committee members, Associate Professor James Brody and Assistant Professor Chang Liu, for their insightful knowledge and access to equipment without which this work would not have been possible.

Thanks to Yi Luo, Samer Kreitem, Tina Chu, and Mingqiu Wang for starting a journey that would not have been, if not for their instruction. I would like to thank Yuting Ji, Yuanqing Xue, Shreya Kumar, Anysa Fernandez, Samantha Michaels, Brandon Szeto, and Thinh Nguyen for joining me in completing that journey.

A special thank you to all Haun lab mates for their help and support during my entire time there. The people of Haun Lab have made the entire endeavor an experience of immense joy.

ABSTRACT

Optimizing Bond Multivalency with Springy Linkers for Therapeutic Nanoparticles

By

Phi Chau Dominh

Master of Science in Biomedical Engineering

University of California, Irvine, 2017

Assistant Professor Jered Haun, Chair

The focus of this paper is optimizing multivalent bond potential between antibody-coated nanoparticles to their respective receptor sites to create a nanoparticle diagnostic/drug/gene delivery system with high targeting efficacy. In recent work with Haun lab, a computational simulation of nanoparticle binding—formally the Nano Adhesive Dynamics (NAD)—was developed to simulate multivalent binding behavior between a nanoparticle decorated with antibodies and a planar surface covered in receptor targets. One of the main findings was that nanoparticles induced large forces on bonds which caused rupture. Rupture was primarily attributed to Brownian motion. Nanospring linker flagelliform—derived from spider silk—and biosensors HP35 and HP35st were chosen for study. HP35 and HP35st were successfully cloned and inserted into a pRS expression vector developed in previous work.

INTRODUCTION

Nanotechnology has gained a wave of momentum these past decades because of its capability to disrupt the current technologies in diagnostic imaging and in therapeutic drug or gene delivery. Nanobiotechnology is described as synthetic structures combined with small biologicals to create hybrid constructs on a molecular level.[1,2] The aim: cure disease by repairing or replacing components of the human cellular system at a molecular level.

Nanobiotechnology has large strides before the technology will mature to a level such as vaccines. But once achieved, nanotechnology promises sensitive biosensors, nanosized microchips for computation, and introducing computer-based logic systems into molecular and DNA structures.[3] This bottom-up approach of medicine can cascade into applications for tissue engineering of muscle, skin, bones, and organs.

The leading therapeutic use for nanobiotechnology is to combat cancer—responsible for the second leading cause of death in the United States. Patients of cancer are not satisfied with current treatments of surgery, chemotherapy, and radiation therapy. Side effects from these treatments are common and contain elevated levels of toxicity. By design, the toxicity and radiation kill cancer cells. This also damages healthy tissues which yield uncomfortable and painful side effects with uncertain repercussions until years after treatment. Nanobiotechnology—specifically nanoparticles—provide a hopeful first step at improving the current treatments. Nanoparticles introduce site-specific targeting while inheriting the potency of current therapeutic agents. The combination would be safer with higher efficacy. The main modalities of a nanoparticle delivery system would be to enhance anticancer agents in tumor

cells than in healthy tissue.[4] The technology has developed extraordinarily rapidly with nanoparticles already playing a role as drug carriers and imaging tools for cancer therapy and detection.[5,6]

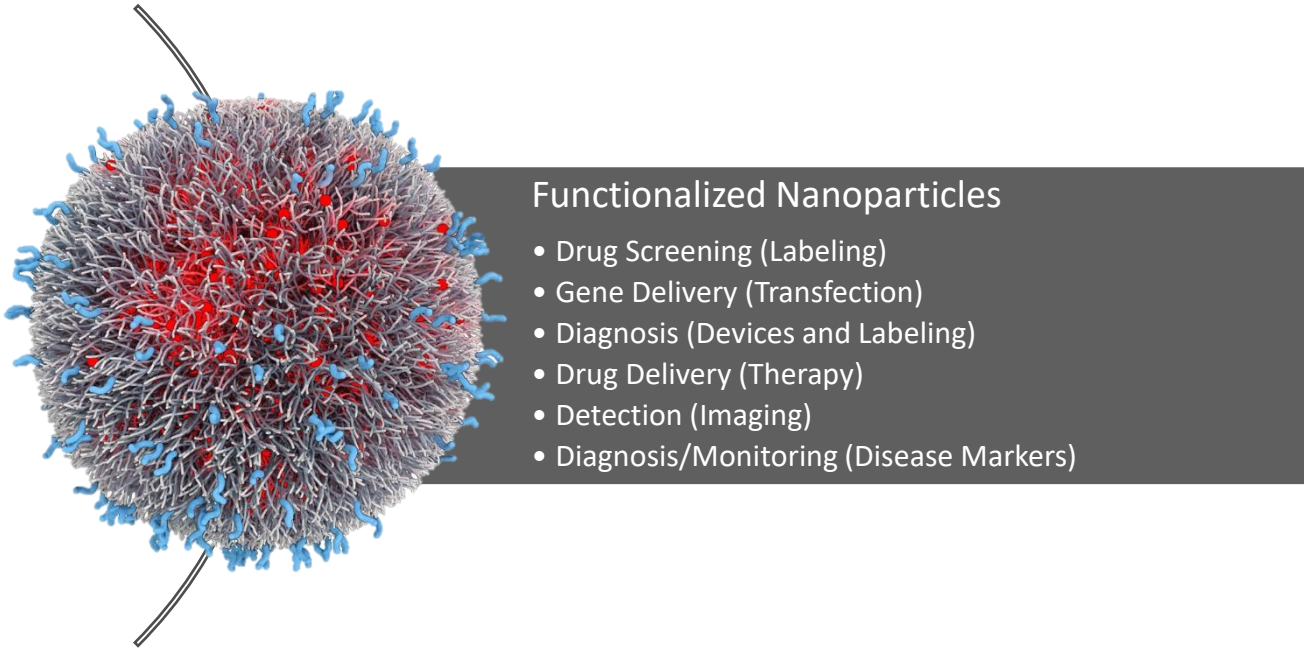

Figure 1. Application of nanoparticles.[1]
Nanoparticles are designed with a modifiable surface of various ligands. The types of ligands can determine whether the nanoparticle is a biosensor, fluorescent tag, imaging, or targeted drug delivery. (Reproduced with modifications)

Nanoparticles can function as a bridge between easily-manufactured common bulk materials and molecular structures. When combined with ligands—such as antibodies—nanoparticles act as drug or gene carriers and facilitate biological functionality to site specific areas of the body.[7–9] Nanoparticles can extend the pharmacokinetics of a drug beyond the effects of just the small-molecule drug alone.[10]

This paper investigates the phenomena of multivalent nanoparticle adhesion and how better to facilitate it. Multivalent binding is described as the capability for a nanoparticle to form multiple ligand-to-receptor contact points with the cell surface. This attribute has been heavily studied and shown to improve targeting of cell types—notably tumor cells.[11–13] Tumor cells can exhibit an increased number of receptors, such as the transferrin receptors, which the respective moiety would selectively bind due to the higher affinity of target receptors (Figure 2).[14] This provides a method to differentiate cancerous cells that may not have unique markers apart from healthy cells of the same cell type.

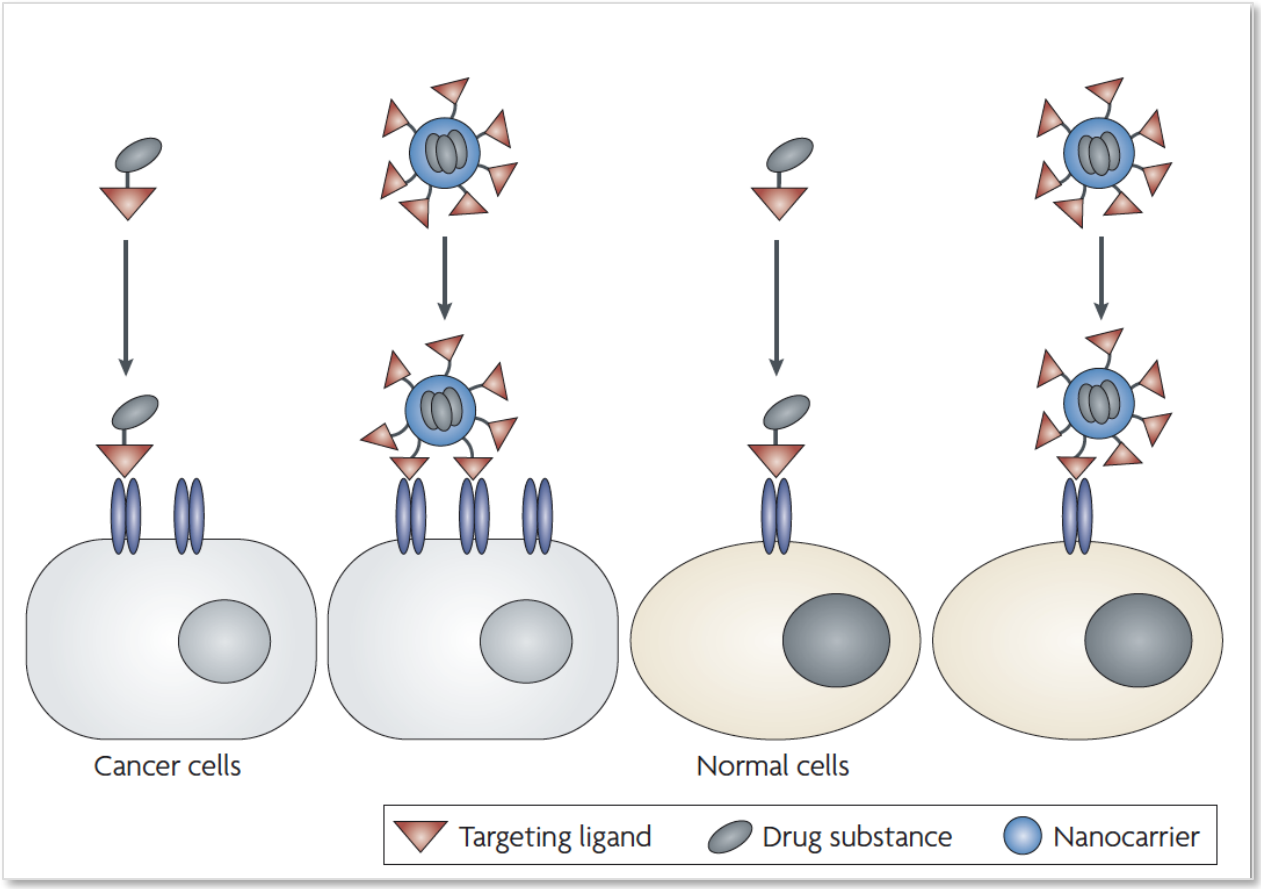

Figure 2. Nanoparticles with numerous targeting ligands can bind to the surface cells multivalency with high receptor density.[10]
When the surface density of the receptor is low on normal cells, the molecular conjugation of a single targeting ligand and a targeted nanoparticle can compete equally since only one ligand-receptor may occur. However, when there is a high surface density of the receptors on cancer cells, the targeted nanoparticle can engage numerous receptors simultaneously to provide enhanced interactions over the one ligand.

To investigate the phenomena and provide a framework for the research we used the Nano Adhesive Dynamics Simulations (NAD). The NAD is a simulation environment that describes the bond dynamics with a nanoparticle sprinkled with antibody ligands and a planar surface decorated with receptor targets. The NAD was used to explore the efficacy of multivalent bonding that we have developed in previous work where all model parameters are known except for bond mechanical properties (reactive compliance, γ, and spring constant, σ).[15–17] The model has shown that the detachment rate (k_D) is not a constant in time. It decreases based on a power law relationships since multivalent particles can form more bonds while bound to the substrate. The time-dependent detachment rate is shown in the following equation:[18]

$$k_D(t) = \frac{k_D^0}{\left({}^{t}/_{t_{ref}}\right)^{\beta}} \tag{1}$$

k_D^0	Detachment rate magnitude
β	Temporal parameter
t_{ref}	Reference time
t	Time

β remains constant over a broad range of antibody and ICAM-1 densities.[19] Equation 1 evolved from the basic rate equation (Equation 2).

$$\frac{\partial B}{\partial t} = k_A C_w - k_D B \tag{2}$$

B	Bound particle density (#/area)
C_w	Unbound particle concentration
k_A	Kinetic rate attachment constant
k_D	Kinetic rate detachment constant
t	time

The NAD model has shown that mechanical force has immense influence over nanoparticle adhesion—or more accurately mechanical work.[18] Bonds were lasting ~0.1 s, where bonds were rupturing under an amount of mechanical work equivalent to the bond chemical energy (Figure 3). For reference, the half-life for antibody/ICAM-1 adhesion—absent of force—is ~100 min. Brownian motion of the nanoparticle was the only significant factor, with a shear force roughly 0.036 pN.[18] Brownian motion, which is linked to particle size, also explains why decreasing particle size increases detachment rate.

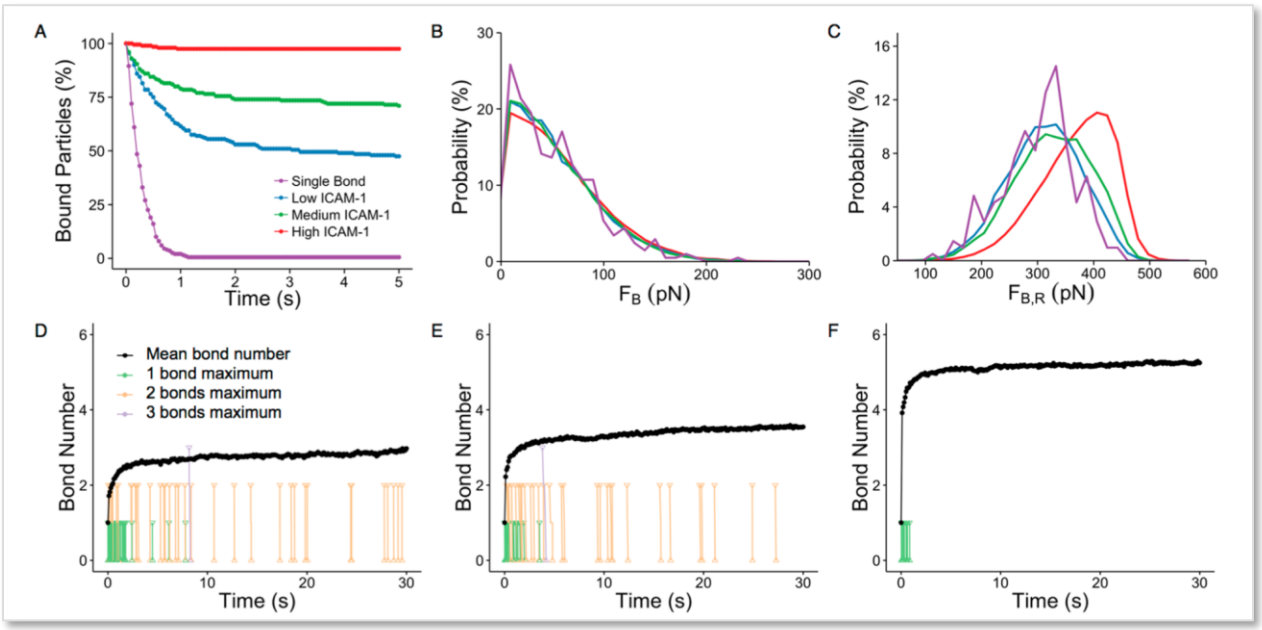

Figure 3. Single-tether simulations and valance-state-dependent detachment dynamics.[18]
(A) Nanoparticles held by a single tether all detached within 1 s, with a profile that closely resembled the initial phase of rapid detachment observed for multivalent cases. (B) The bond force distribution for the single-tether simulation was nearly identical to the multivalent cases. (C) Bond rupture force distributions were similar between the single tether and low ICAM-1 density cases, but the rupture force shifted to higher values with increased valency. (D-F) Valence-state-dependent detachment dynamics. The mean bond number (black line) is shown over time at low antibody density and either (D) low, (E) medium, or (F) high ICAM-1 density. All detachment events are included in the plot and color-coded on the basis of the maximum bond number achieved: one bond (green), two bonds (orange), or three bonds (purple). The point of detachment is indicated by the triangle (Δ), and lines then trace back up to the time point at which that nanoparticle was at its maximum bond nu8mber, which is indicated by an upside-down triangle (∇). Nanoparticles restricted to a single bond detached rapidly, most within the first few seconds. Nanoparticles that detached from the second and third bond states persisted longer and quickly dropped all the way to zero bonds, typically within 0.1 s, limiting the chance for bonds to reform.

Bond force (F_B) and rupture force ($F_{B,R}$) were studied with variable reactive compliance (γ) and spring constants (σ) in Figure 4 and Table 1. Average $F_{B,R}$ was ~290 pN with a bond lifetime of ~0.25 s.[18] Bonds would rupture when mechanical work exceeded ~$\sigma\gamma^2$ where best fits were $\gamma = 0.27$ nm and $\sigma = 0.8$ N/m. A better fit could be possible if σ were more adjustable.

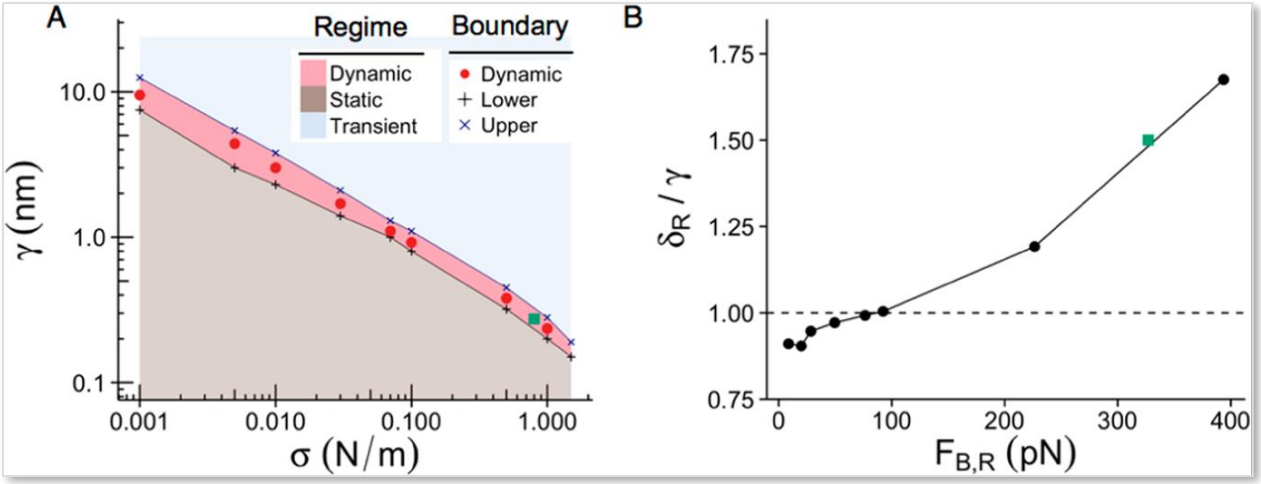

Figure 4. Mechanical state diagram.[18]
(A) Nanoparticle detachment dynamics at low antibody and medium ICAM-1 densities, assessed across a large range of $\boldsymbol{\gamma}$ and $\boldsymbol{\sigma}$ values. The transient regime (blue) corresponds to highly unstable adhesion, defined as <5% of nanoparticles remaining bound after 5 s. the static regime (brown) corresponds to highly stable adhesion, with <95% remaining bound after 5 s. The dynamic regime (red) lies in between, and the red circles indicate the mechanical property combinations that precisely matched experiments. (B) The bond rupture length ($\boldsymbol{\delta_R}$) was slightly less than $\boldsymbol{\gamma}$ at low $\boldsymbol{F_{B,R}}$ exceeded ~95 pN. Teal squares denote the matching condition using $\boldsymbol{\gamma}$ measured with optical tweezers force spectroscopy experiments (0.27 nm) and the best fit $\boldsymbol{\sigma}$ (0.8 N/m).

Table 1. Different y and sigma Combinations Resulting in Nanoparticle Dynamics That Match Experimental Results

$\boldsymbol{\sigma}$ (N/m)	$\boldsymbol{\gamma}$ (nm)	$\boldsymbol{\beta}$	$\boldsymbol{k_D^0}$ (ms^{-1})	$\boldsymbol{F_{B,R}}$	$\boldsymbol{\delta_R}$	Rupture work (pN·nm)
0.001	9.5	0.77 ± 0.02	140 ± 10	8.6	8.6	81.7
0.005	4.4	0.75 ± 0.03	140 ± 10	19.9	4.0	87.6
0.01	3	0.81 ± 0.02	90 ± 10	28.4	2.8	85.2
0.03	1.7	0.78 ± 0.03	90 ± 10	49.5	1.7	84.2
0.07	1.1	0.75 ± 0.03	100 ± 10	76.4	1.1	84.0
0.1	0.92	0.79 ± 0.02	110 ± 10	92.3	0.9	84.9
0.5	0.38	0.74 ± 0.03	150 ± 10	226.4	0.5	86.0
0.8	0.27	0.78 ± 0.04	47 ± 6	324.4	0.4	87.6
1	0.24	0.75 ± 0.02	120 ± 10	393.7	0.4	94.5

The objective of this paper is to investigate whether these flexible fusion proteins would increase spring constant (σ) without affecting the reactive compliance (γ). Experimentally, this would increase the contact time of an initial bond long enough for sister bonds to form and improve the efficacy of nanoparticle multivalent binding.

The NAD showed that a better model could be developed if spring constant (σ) could be increased. A novel solution would use a nanospring to dampen the effects of Brownian motion and reduce mechanical forces (Figure 5).[20]

Figure 5 introduces flagelliform and GGS linkers. These are nanospring linkers that would, in theory, reduce the mechanical strain of Brownian motion and optimize the case for multivalent bonding.

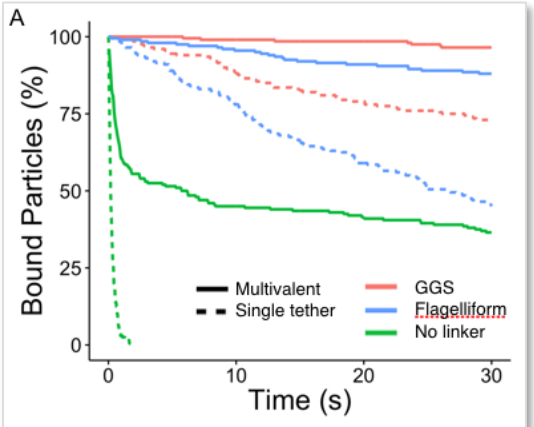

B

Linker	$k_{r,1}$ (s^{-1})	$F_{B,R}$ (pN)	Δx (nm)	β	k_D^0 (s^{-1})
None	3.8	290	0.1	0.78	0.102
GGS	0.012	280	4.8	NA	NA
Flagelliform	0.026	275	0.4	0.08	0.005

Figure 5. Effect of peptide linkers.[20]
(A) Detachment profiles for multivalent and single tether cases. (B) Key bond and nanoparticle detachment metrics.

Brenner *et al*. has demonstrated that the peptide motif GPGGA (flagelliform)[21] behaves as a linear nanospring spring and can measure intracellular tension forces when combined with Förster resonance energy transfer (FRET).[22,23]

Along with the nanospring protein, we are interested in using HP35 and a stable mutant HP35st as linker proteins. Both are ultrafast-folding peptides that undergo an equilibrium unfolding/folding transition in response to forces of 7 pN and 10 pN, respectively.[24] But whereas flagelliform behaves as a linear spring, HP35 and HP35st exist in only two states: relaxed and extended.

Flagelliform

Flagelliform, in its natural form, is known as spider capture silk. It readily outperforms almost any synthetic material in strength and elasticity, with a tensile strength of ~1 GPa with comparable strength to Kevlar[21] or steel[25]. It's repeating structural motif of GPGGA[21] (Figure 6) gives it an elasticity that stretches as much as 500—1,000%.[26,27] Strain on the nanospring can be measured when combined with FRET.[23]

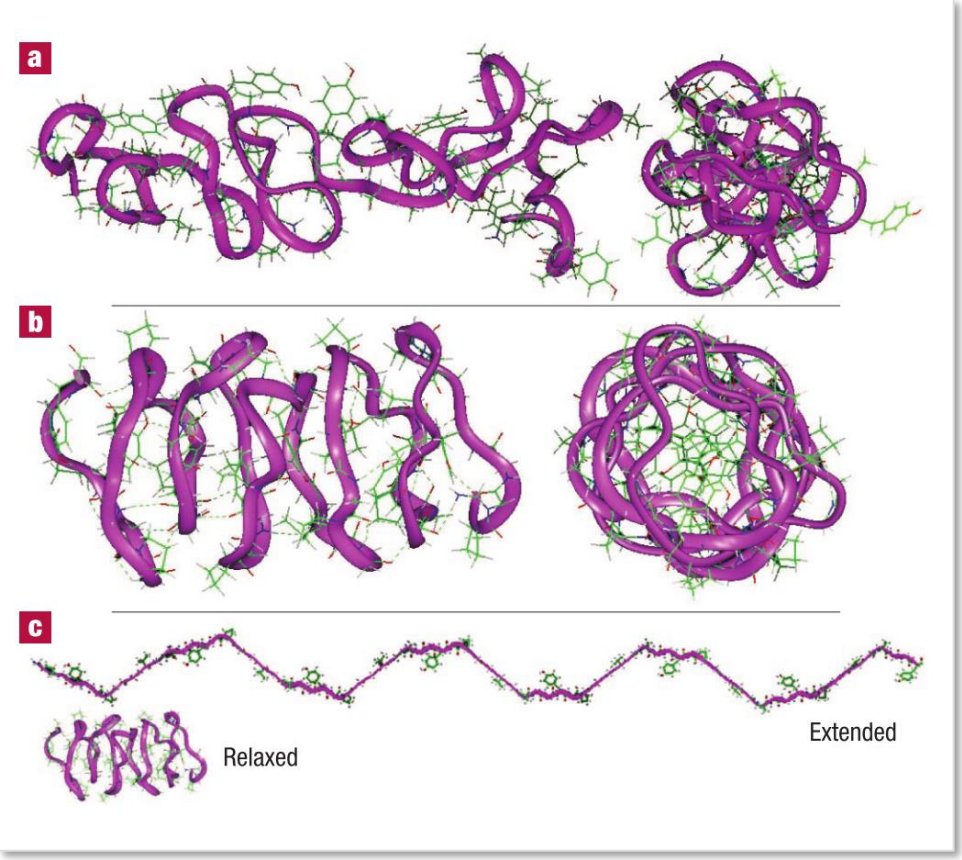

Figure 6. Molecular models for relaxed and extended flagelliform protein sequences from spider capture silk.[33]
a, b, Side and end views for possible flagelliform protein conformations of (**a**) *Araneus gemmoides*, 85 amino acids long (sequence is VGPGGAYGPGGVYGPGAGGLSGPGGAGPYGPGGVGPGGAGPYGPGGVGPGGAGPYGPGGVG PG GAGPYGPGGVGPGGAGPYGPGG), and (**b**) *Nephila clavipes*[33], 75 amino acids long, $(GPGGX)_{15}$, where X is Y or V, alternately. **c**, Scale models for extended and relaxed GPGGX sequences, 75 amino acids long. The extended model is at the maximu8m extension of the protein, without deforming bond angles.

FRET

FRET is a mechanism that entails energy transfer between two fluorophores.[28] This an extremely sensitive method to measure changes in small distances such as distances between domains in a single protein and interactions between proteins.[29–31] An excited fluorophore emits a virtual photon that is absorbed by a receiving fluorophore and the efficiency of the transfer is measured (Figure 7).

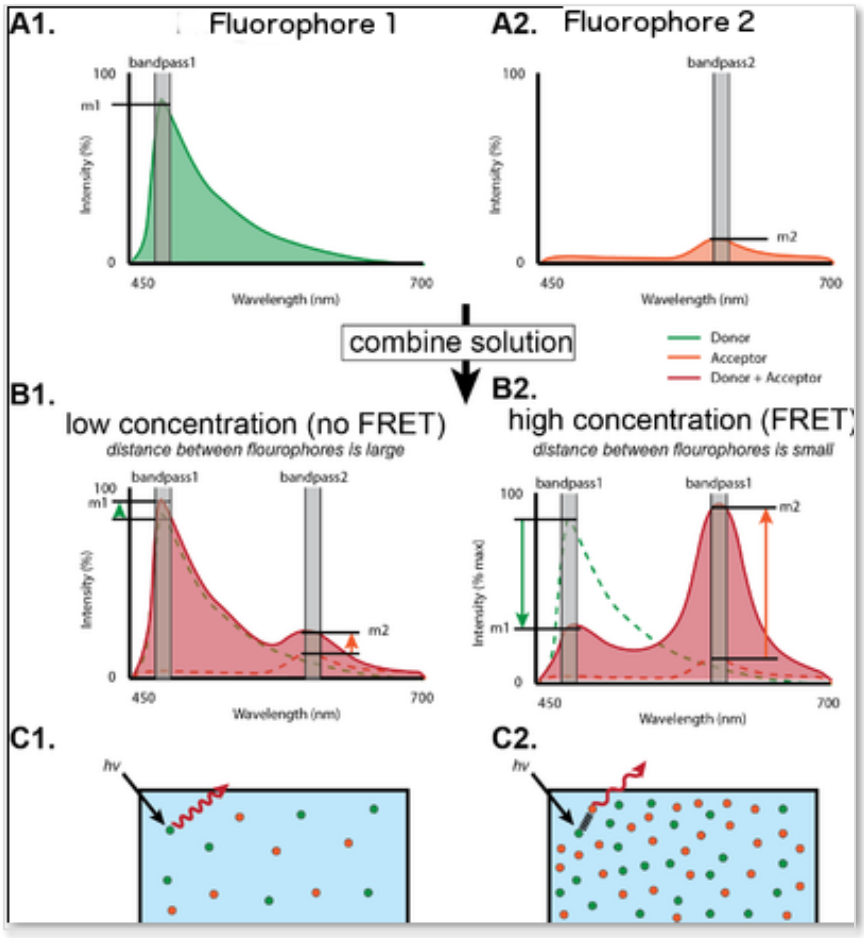

Figure 7. Cartoon diagram of the concept of Förster resonance energy transfer (FRET).[34]
A, Two hypothetical fluorophores that fluoresce at two different wavelengths. **B1**, When these fluorophores are mixed at low concentrations there is little FRET (low FRET efficiency) because the distance between fluorophores is high. **B2**, At high concentrations the distance between fluorophores is small resulting in high FRET efficiency. **C**, Diagram demonstrating the mechanism of FRET

Tension biosensors HP35 and HP35st were engineered by Austen *et al.* to study the pN molecular forces 6—8 pN and 9—11 pN, respectively, in tissue rigidity.[24] The biosensors are sharp, very fast, and reversible in force responses that fully unravel at 35 pN (Figure 8).

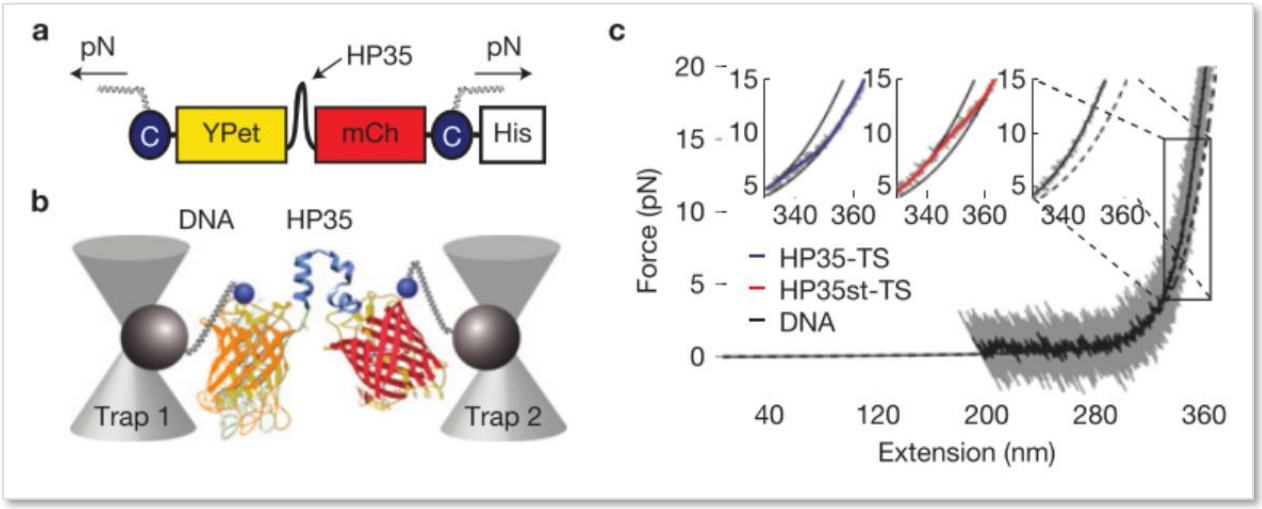

Figure 8. Biosensor calibration using single-molecule force spectroscopy.[24]
(**a**) HP35-TS comprises two fluorophores, YPet and mCherry (mCh), which are linked by the villin headpiece peptide (HP35). Mechanical force across this biosensor leads to HP35 unfolding, increase in fluorophore separation distance and reduced FRET. For single-molecule calibration, DNA handles were attached using cysteines (C), a His-tag was used for purification. (**b**) Schematic illustration of the dual-trap optical tweezer set-up used for calibration. (**c**) 200 kHz resolution force-extension trace (grey) fitted with an extensible worm-like chain model (black). Inset: zoom into representative force-extension traces of individual HP35(st)-TS molecules as compared to DNA; the fit to HP35-TS data is shown in blue, HP35st-TS in red and DNA in black.

pRS-4420 Plasmid

The pRS-4420 plasmid was developed from previous work in yeast secretion (Figure 9). The plasmid was designed with a recombinant protein domain between the single chain antibody 4420 and fluorophore mCherry using *BSiWI* and *MluI* restriction enzymes (APPENDIX). The flexible linkers would be cloned into this region. But feasibly, the region can be expanded to insert another single chain antibody or I-domain integrin that were developed in a previous study.

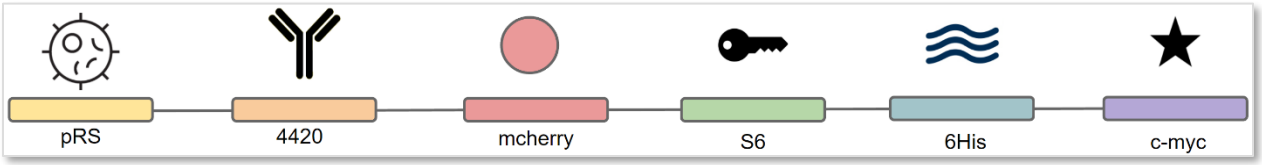

Figure 9. Schematic of pRS-4420 plasmid.

(*from left to right)* pRS plasmid backbone for yeast secretion, 4420 is antibody region, mCherry is fluorophore, S6 peptide tag is an orthogonal binding site for attaching to a nanoparticle via an enzymatic reaction[35], 6His for protein purification, c-Myc as a ligand binding site.

RECOMBINANT PLASMID CONSTRUCTION OF NANOSPRINGS AND HP35 FLEXIBLE LINKERS

Inserts for flagelliform, GGS control linker protein, HP35, and HP35st were generated through a combination of annealing oligonucleotides and gBlocks® gene fragments purchased through Integrated DNA Technologies (IDT). The control GGS control linker protein consists of repeat motif glycine-glycine-serine.

Flagelliform and GGS

Flagelliform (flag50) and GGS (ggs50) were generated using IDT gBlocks®. The proteins are designed to be 50 amino acids in length. The sequence below describes flag50 which includes *MluI* and *BSiwI* restriction sites (highlighted), followed by ggs50.

flag50

5'— TAA TTA TGA AAC ATA TTA TTA CGC GTG GGC CAG GGG GTG CCG GTC CGG GAG GGG CAG GTC CAG GAG GTG CGG GCC CCG GGG GAG CGG GCC CTG GGG GAG CGG GTC CGG GCG GCG CAG GAC CCG GAG GCG CGG GTC CTG GTG GAG CAG GCC CTG GAG GAG CCG GCC CGG GTG GCG CAC GTA CGT AAA CAA ACC TTA TAA TTA T –3'

ggs50

5'— GGA TTC ACT TAC GCG TGG CGG CAG TGG AGG CAG CGG CGG TAG TGG TGG ATC AGG AGG CAG TGG GGG ATC CGG CGG AAG CGG TGG GTC TGG AGG ATC AGG TGG GTC TGG CGG GAG CGG TGG GAG TGG GGG GAG CGG TGG CTC TGG GGG TTC TGG TGG TTC AGG CGG CCG TAC GGT TAT GAC TCA AA –3'

HP35 and HP35st

Inserts HP35 and HP35st were created by annealing oligonucleotides. The 5'—3' forward sequences for HP35 and HP35st are described below and annealed with their respective reverse sequences. The differences between HP35 and HP35st are underlined.

HP35

5'— CTC TCC GAT GAG GAC TTC AAA GCT GTG TTT GGC ATG ACC AGG AGC GCA TTT GCC AAC CTT CCT CTG TGG AAA CAG CAA CAC CTG AAG AAG GAA AAG GGA CTG TTC –3'

HP35st

5'— CTC TCC GAT GAG GAC TTC AAA GCT GTG TTT GGC ATG ACC AGG AGC GCA TTT GCC AAC CTT CCT CTG TGG AAA CAG CAA GCT CTG ATG AAG GAA AAG GGA CTG TTC—3'

These inserts were extended with *MluI* and *BsiWI* using extension PCR with the following forward and reverse primers. The same primer could be used for both sequences since the primer overlapping region is the same for both.

MluI-HP35-fwd

5'— GAG GAG ACG CGT CTC TCC GAT GAG GAC TTC AA –3'

HP35-bsiw-rev

5'— CTC CTC CGT ACG GAA CAG TCC CTT TTC CTT C –3'

RESULTS

HP35, HP35st, and pRS-4420 was digested with *MluI* and *BsiWI*. Inserts HP35 and HP35st were then purified with a QIAquick PCR Purification Kit (Qiagen) with concentrations 89.3 µL/ng and 56.7 µL/ng, respectively. pRS-4420 plasmid was purified using gel electrophoresis.

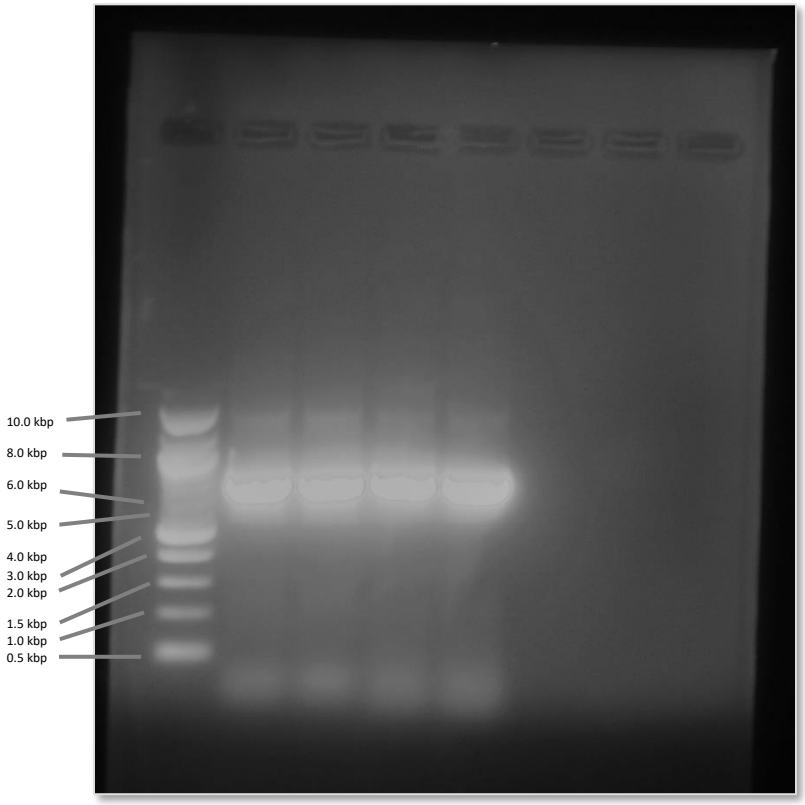

Figure 10. pRS-4420 Digest.
pRS-4420 plasmid digested with restriction enzymes *MluI* and *BsiWI* and gel purified. Expected size is ~7.3 kbp. (*from left to right*) 1 kb ladder (NEB), digested pRS-4420 plasmid 1—4.

Inserts HP35 and HP35st were ligated to pRS-4420 and grown on LB Amp plates. Figure 11 shows colony growth after 24 h incubation.

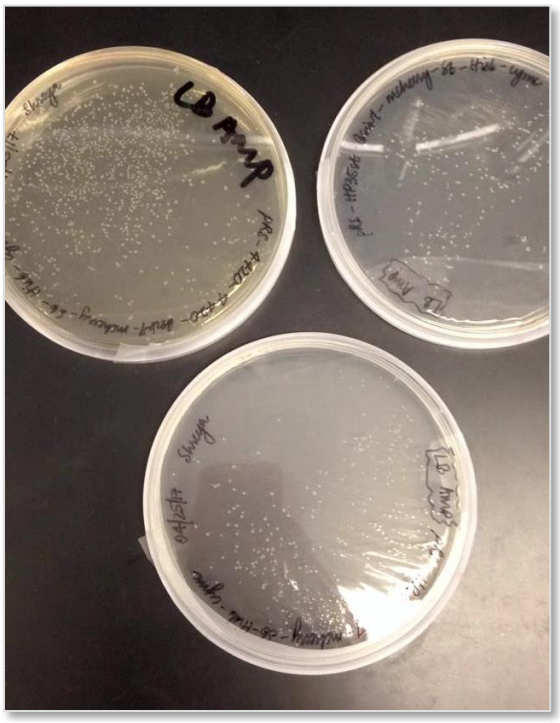

Figure 11. 24h Colony Growth.
pRS-4420-HP35 and pRS-4420-HP35st colony growth after 24h. pRS-4420-4420 also shown in the figure (detailed in FUTURE DIRECTION)

HP35 and HP35st have been succesfully cloned into pRS-4420, confirmed with sequencing via GENEWIZ.

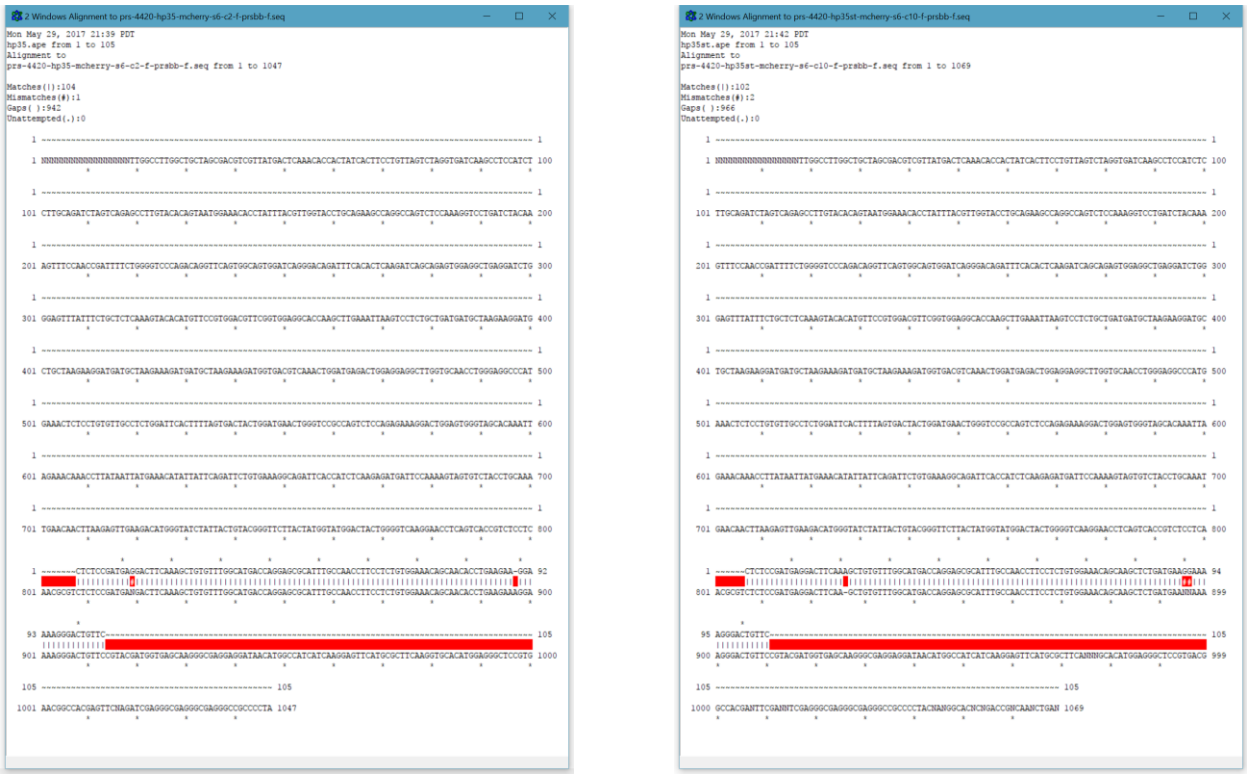

Figure 12. Sequence Results

Sequence results of pRS-4420-HP35 (*left*) and pRS-4420-HP35st (*right*). DNA was sequenced by GENEWIZ

FUTURE DIRECTION

flag50 and ggs50 have been obtained and will be immediately digested and ligated with pRS-4420 due to the complications of cloning multiple repeat sequences[32].

The pRS-4420 plasmid design allowed for flexibility in construct generation. As alluded in Figure 11, this would allow different peptides to be inserted. Other antibodies may be used to further study bond energy and reactive compliance (γ) and how these linkers may affect them.

Theoretically, placement of these linker peptides should not affect γ nor spring constant σ. But testing insertion sites behind mCherry and further beyond the construct would warrant future.

REFERENCES

1. McNeil, S. E. Nanotechnology for the biologist. *J. Leukoc. Biol.* **78,** 585–594 (2005).

2. Fortina, P., Kricka, L. J., Surrey, S. & Grodzinski, P. Nanobiotechnology: The promise and reality of new approaches to molecular recognition. *Trends in Biotechnology* **23,** 168–173 (2005).

3. Liu, Y., Miyoshi, H. & Nakamura, M. Nanomedicine for drug delivery and imaging: A promising avenue for cancer therapy and diagnosis using targeted functional nanoparticles. *International Journal of Cancer* **120,** 2527–2537 (2007).

4. Orive, G., Hernández, R. M., Gascón, A. R., Domínguez-Gil, A. & Pedraz, J. L. Drug delivery in biotechnology: Present and future. *Current Opinion in Biotechnology* **14,** 659–664 (2003).

5. Roco, M. C. Nanotechnology: Convergence with modern biology and medicine. *Current Opinion in Biotechnology* **14,** 337–346 (2003).

6. Brigger, I., Dubernet, C. & Couvreur, P. Nanoparticles in cancer therapy and diagnosis. *Adv. Drug Deliv. Rev.* **64,** 24–36 (2012).

7. Akerman, M. E., Chan, W. C. W., Laakkonen, P., Bhatia, S. N. & Ruoslahti, E. Nanocrystal targeting in vivo. *Proc. Natl. Acad. Sci. U. S. A.* **99,** 12617–12621 (2002).

8. Kim, T. & Hyeon, T. Applications of inorganic nanoparticles as therapeutic agents. *Nanotechnology* **25,** 12001 (2014).

9. Zhu, M., Nie, G., Meng, H. & Xia, T. Physicochemical properties determine nanomaterial cellular uptake, transport, and fate. *Acc. Chem. Res.* **46,** 622–631 (2012).

10. Davis, M. E., Chen, Z. G. & Shin, D. M. Nanoparticle therapeutics: an emerging treatment modality for cancer. *Nat. Rev. Drug Discov.* **7,** 771–782 (2008).

11. Hilgenbrink, A. R. & Low, P. S. Folate receptor-mediated drug targeting: From therapeutics to diagnostics. *Journal of Pharmaceutical Sciences* **94,** 2135–2146 (2005).

12. Lu, Y. & Low, P. S. Folate-mediated delivery of macromolecular anticancer therapeutic agents. *Advanced Drug Delivery Reviews* **64,** 342–352 (2012).

13. Salmaso, S. *et al.* Specific antitumor targetable β-cyclodextrin-poly(ethylene glycol)-folic acid drug delivery bioconjugate. *Bioconjug. Chem.* **15,** 997–1004 (2004).

14. Gatter, K. C., Brown, G., Trowbridge, I. S., Woolston, R. E. & Mason, D. Y. Transferrin receptors in human tissues: their distribution and possible clinical relevance. *J. Clin. Pathol.* **36,** 539–545 (1983).

15. Haun, J. B., Robbins, G. P. & Hammer, D. A. Engineering Therapeutic Nanocarriers with Optimal Adhesion for Targeting. *J. Adhes.* **86,** 131–159 (2010).

16. Wang, J., Tian, S., Petros, R. A., Napier, M. E. & Desimone, J. M. The complex role of

multivalency in nanoparticles targeting the transferrin receptor for cancer therapies. *J. Am. Chem. Soc.* **132,** 11306–11313 (2010).

17. Haun, J. B., Pepper, L. R., Boder, E. T. & Hammer, D. A. Using engineered single-chain antibodies to correlate molecular binding properties and nanoparticle adhesion dynamics. *Langmuir* **27,** 13701–13712 (2011).

18. Wang, M., Ravindranath, S. R., Rahim, M. K., Botvinick, E. L. & Haun, J. B. Evolution of Multivalent Nanoparticle Adhesion via Specific Molecular Interactions. *Langmuir* **32,** 13124–13136 (2016).

19. Haun, J. B. & Hammer, D. A. Quantifying nanoparticle adhesion mediated by specific molecular interactions. *Langmuir* **24,** 8821–8832 (2008).

20. Haun, J. B. *Project Description*. (2016).

21. Hinman, M. B., Jones, J. A. & Lewis, R. V. Synthetic spider silk: A modular fiber. *Trends in Biotechnology* **18,** 374–379 (2000).

22. Brenner, M. D. *et al.* Spider Silk Peptide Is a Compact, Linear Nanospring Ideal for Intracellular Tension Sensing. *Nano Lett.* **16,** 2096–2102 (2016).

23. Evers, T. H., Van Dongen, E. M. W. M., Faesen, A. C., Meijer, E. W. & Merkx, M. Quantitative understanding of the energy transfer between fluorescent proteins connected via flexible peptide linkers. *Biochemistry* **45,** 13183–13192 (2006).

24. Austen, K. *et al.* Extracellular rigidity sensing by talin isoform-specific mechanical linkages. *Nat. Cell Biol.* **17,** 1597–1609 (2015).

25. Weast, R. C. *CRC handbook of chemistry and physics*. *CRC Press* (1972).

26. Opell, B. D. & Bond, J. E. Capture thread extensibility of orb-weaving spiders: testing punctuated and associative explanations of character evolution. *Biol. J. Linn. Soc.* **70,** 107–120 (2000).

27. Köhler, T. & Vollrath, F. Thread biomechanics in the two orb-weaving spiders Araneus diadematus (Araneae, Araneidae) and Uloborus walckenaerius (Araneae, Uloboridae). *J. Exp. Zool.* **271,** 1–17 (1995).

28. Cheng, P.-C. in *Handbook Of Biological Confocal Microscopy* 162–206 (2006). doi:10.1007/978-0-387-45524-2_8

29. Harris, D. C. *Quantitative chemical analysis*. (W.H. Freeman and Co, 2010).

30. Truong, K. & Ikura, M. The use of FRET imaging microscopy to detect protein-protein interactions and protein conformational changes in vivo. *Curr. Opin. Struct. Biol.* **11,** 573–8 (2001).

31. Pollok, B. A. & Heim, R. Using GFP in FRET-based applications. *Trends Cell Biol.* **9,** 57–60 (1999).

32. Hommelsheim, C. M., Frantzeskakis, L., Huang, M., Ülker, B. & Salas, M. PCR amplification of repetitive DNA: a limitation to genome editing technologies and many other applications. *Sci. Rep.* **4,** 5052 (2015).

33. Becker, N. *et al.* Molecular nanosprings in spider capture-silk threads. *Nat. Mater.* **2,** 278–283 (2003).

34. Neveu, C. File:Concept of FRET.png - Wikimedia Commons. Available at: https://commons.wikimedia.org/wiki/File:Concept_of_FRET.png. (Accessed: 29th May 2017)

35. Zhou, Z. *et al.* Genetically Encoded Short Peptide Tags for Orthogonal Protein Labeling by Sfp and AcpS Phosphopantetheinyl Transferases. *ACS Chem. Biol.* **2,** 337–346 (2007).

APPENDIX

pRS-4420 Construct

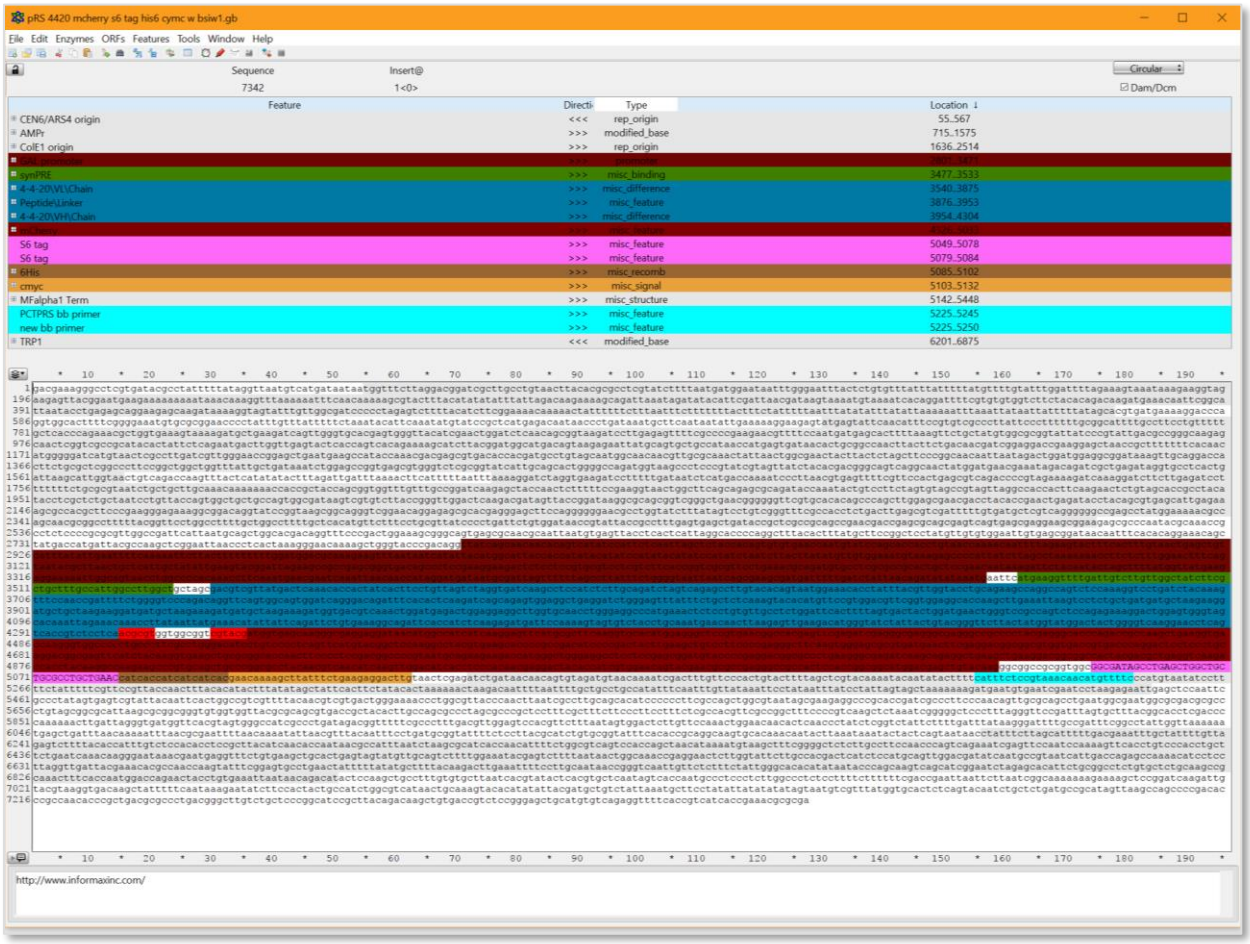

Figure 13. pRS-4420 construct.

pRS-4420 construct with *BSiWI* and *MluI* restriction enzymes highlighted in bright red.

Materials and Methods

Reagents, Materials, and Kits

All materials and reagents used in this paper are listed in the following table:

Table 2 Reagents, materials, and kits applied in plasmid construction

Reagents	*Company*
Restriction enzyme MluI	New England Biolabs
Restriction enzyme BsiwI	New England Biolabs
100 bp DNA ladder	New England Biolabs
1 kb DNA ladder	New England Biolabs
T4 DNA ligase	New England Biolabs
Vent DNA polymerase	New England Biolabs
SOC outgrowth medium	New England Biolabs
Gel loading dye	New England Biolabs
Agarose	Invitrogen
TAE	Invitrogen
Ethidium bromide	Invitrogen
LB Broth Base	Invitrogen
LB Agar powder	Invitrogen
Ampicillin	Invitrogen
PCR tubes	
Razor blades	Fisher Scientific
QIAquick Gel Extraction Kit	Qiagen
QIAquick PCR Purification Kit	Qiagen
QIAprep Spin Miniprep Kit	Qiagen

Strains and Media

Escherichia coli strain DH5α (New England Biolabs) was used for recombinant plasmids gene cloning. Luria-Bertani (LB) medium (10.0 g/L tryptone, 5.0 g/L yeast extract, 10.0 g/L NaCl, pH 7.5, supplemented with 50 mg/mL ampicillin) was used for bacterial growth and plasmid amplification. LB agar plates (10.0 g/L peptone, 5.0 g/L yeast extract, 5.0 g/L NaCl, 12.0 g/L agar, supplemented with 50 mg/mL ampicillin) was used for bacterial growth and selection.

PCR (typical protocol using Vent Polymerase)

PCR Master Mix (50 µL Volume)

Thermopol Buffer	5 µL
Vent Polymerase	1 µL
dNPTs	1 µL
Forward Primer (100 mM)	1 µL
Reverse Primer (100 mM)	1 µL
Template DNA	1 µL
Ultrapure Water	to 50 µL

PCR Thermocycling

Initial Denature	94°C	2 min
25x Cycle Denature	94°C	30 sec
25x Annealing	55-62°C	30 sec
25x Extension	72°C	45 sec
Final Extension	72°C	5 min
Storage	4°C	∞

Electrophoresis and Gel Extraction

GEL PREPARATION AND EXTRACTION PROTOCOL

1	Prepare 0.5 g agarose (or 1 g low-melting temperature agarose) in 50 mL TAE.
2	Melt agarose in microwave for approximately 30 s. Concurrently for 10 s until solution is clear of agarose particles.
3	Cool solution with water bath until warm to the touch.
4	Pour solution into gel slab, mix 2.5 µL ethidium bromide, and add gel comb.
5	Dilute sample with loading buffer and add to gel (30 µL for 8 well, 10 µL for 15 well).
6	Separate samples with an empty lane unless the product sizes are well separated.
7	Run at 120V for 45 min (1%) or 1.5 hrs (2%).
8	Cut bands out with clean razor blade and place into microcentrifuge tube.
9	Extract the bands using the QIAquick Gel Extraction Kit.

Restriction Enzyme Digestion

Typical Restriction Digestion Master Mix (50 µL Volume)

Restriction Enzyme(s)	10 units or 1 µL per enzyme
DNA	1 µg
NEBuffer (10x)	5 µL
Ultrapure Water	To 50 µL
Incubation Temperature	37°C, 55°C, or per enzyme specification
Incubation Time	Overnight for 12 hrs* or per enzyme specification

*If no star activity is present in either enzyme

If sequential digestion is to be performed:

1. Incubate with lower temperature enzyme first overnight for 12 hrs (if no star activity) or per enzyme specification. Heat inactivate per enzyme specification.
2. Add second enzyme and incubate overnight for 12 hrs (if no star activity) or per enzyme specification. Heat inactivate per enzyme specification

Purify vectors using electrophoresis followed by QIAquick Gel Extraction Kit. Purify inserts using Qiagen PCR clean-up kit.

Ligation (typical protocol using T4 DNA Ligase)

Ligation Master Mix (20 µL Volume)

*T4 DNA Ligase Buffer (10x)**	10 units or 1 µL per enzyme
T4 DNA Ligase	1 µL
Vector DNA	~10-50 ng
Insert DNA	Variable**
Ultrapure Water	To 20 µL
Incubation Temperature	Room Temperature
Incubation Time	4 hrs

**T4 DNA Ligase Buffer should be thawed and resuspended at room temperature. Stock T4 DNA Ligase Buffer should be aliquoted.*

***Maintain a 3:1 insert:vector molar ration.*

Gently mix reaction by pipetting up and down. Heat inactivate at 65°C for 10 minutes. Chill on ice and prepare to transform into 50 µL competent cells.

Transformation into E. coli (DH5α from Invitrogen)

E. COLI CELL TRANSFORMATION PROTOCOL	
1	Add 2 µL ligation mixture to 50 µL DH5α cells, let sit for 30 min on ice.
2	Heat shock for 45 sec at 42°C, place back on ice for 2 min.
3	Add 0.95 mL SOC media.
4	Incubate at 37°C for 1 hr.
5	Centrifuge cells down and aspirate ~900 µL, resuspend cells in remaining media.
6	Plate cells onto LB-Amp plates.

Colony PCR

COLONY PCR PROTOCOL	
1	Identify single colonies and scrape into 50 µL sterile ultrapure water using a sterile O-ring scraper
2	Perform typical Vent PCR at ½ volume with 5 µL of cell suspension.
3	Check for product on a 1% agarose gel following gel preparation protocol.
4	Positive samples can be plated (5 µL) and grown (remaining 40 µL) in 3 mL LB Amp broth for later use and sequencing, respectively.

Media Recipes

LB Broth:

Base media (for 1 L): 25 g LB powder into water, filter sterilize or autoclave.

Supplement: Add ampicillin or other antimicrobial agent (typical concentration of 50 mg/mL) once the media has cooled to ~50°C (touchable by bare hand).

LB Plates:

Base media: 40 g LB agar powder/L into water, autoclave.

Supplements: Add ampicillin or other antimicrobial agent (typical concentration of 50 mg/mL) once the media has cooled to ~50°C (touchable by bare hand).

Pour into individual plates, ensuring no bubble formation.